Anti-Disturbance Cooperative Fuzzy Tracking Control of Multi-PMSMs Low-Speed Urban Rail Traction Systems *

Yuchen Dai[1], Liyan Zhang[1] (IEEE Member), Qihong Chen[1] (IEEE Member), Dezhi Xu[2,†] (IEEE Senior Member), Xing-Gang Yan[3]

[1]School of Automation, Wuhan University of Technology, Wuhan, 430070, China

[2]School of Internet of Things Engineering, Jiangnan University, Wuxi, 214122, China

[3]School of Engineering and Digital Arts, University of Kent, Canterbury, CT2 7NT, U.K.

Abstract: A directed-graph-based cooperative control scheme is proposed, to improve the synchronization performance and reduce its error under disturbance between multiple permanent magnet synchronous traction motors in low-speed urban rail transit. First, each motor is supposed to an agent of multi-agent system, and the information between multiple motors can be transmitted through communication topology network, which ensure the consistency of the response of each agent. Then, considering that the load torque of the motor is disturbed during operation, a finite-time disturbance-observer is proposed to estimate the unknown load disturbance, thus guarantee the anti-disturbance ability of the system. Besides, the nonlinear parts of the dynamic model are approximated by fuzzy logic systems, and a second-order sliding mode differentiator is designed to avoid the direct derivation of virtual control law and the problem of differential explosion. Finally, the system is proved to be finite-time stable. The feasibility and effectiveness of the proposed control scheme are verified by the hardware-in-the-loop platform.

Keywords: low-speed urban rail transit; traction system; multiple permanent magnet synchronous motors; directed-graph; disturbance-observer; cooperative control.

*This work was partially supported by National Key Research and Development Program of China (2019YFB1504703), National Natural Science Foundation of China (61973140,62173264), and China Scholarship Council (202106950045).

†Corresponding author: E-mail: lutxdz@126.com (D. Xu).

Nomenclature

$i_{i.d}$, $i_{i.q}$	$d-q$ axis stator currents
$u_{i.d}$, $u_{i.q}$	$d-q$ axis stator voltages
R_s	Armature resistance
L_s	Stator inductance
φ_f	Permanent magnet flux
p	Number of pole pairs
$T_{i.m}$	Electromagnetic torque
J	Equivalent inertia
F	Viscous friction of the rotor
V_{dc}	DC catenary voltage
$\omega_{i.g}$	Rotor angular speed
$T_{i.L}$	Load torque
$T_{i.d}$	Disturbance torque
G	Directed-graph of multi-agent systems
$\mathscr{V}$	Set of nodes
$\mathscr{Y}$	Set of edges
A	Adjacency matrix
a_{ij}	Weighted coefficient between node i and node j
L	Laplacian matrix
l_{ij}	Element of Laplacian matrix
D	In-degree matrix
d_i	In-degree of node
B	Diagonal matrix
b_i	Weighted coefficient between leader and node
$W_{i.2}$, $W_{i.3}$	Unknown idea parameter vectors

$\partial_{i.2}$, $\partial_{i.3}$	Fuzzy basis function vectors
$\kappa_i(x)$	Gaussian functions
$\alpha_{i.1d}$, $\alpha_{i.2d}$	Control gains of disturbance-observer (DO)
$\tilde{\phi}_{i.\delta}$	Observation error of DO
x_1^c	Desired angular speed
$e_{i.1}$	Angular speed tracking error
$z_{i.1}$	Neighborhood synchronization error
$z_{i.2}$, $z_{i.3}$	Current tracking errors
$x_{i.2}^d$	Virtual control law
$x_{i.2}^c$, $x_{i.3}^c$	Reference value of $d-q$ axis currents
$\sigma_{i.1}$, $\sigma_{i.2}$	Control gains of second-order sliding mode differentiator (SOSMD)
ξ_i	Error compensating signal
$\bar{z}_{i.1}$	Compensated tracking error
$S_{i.q}$, $S_{i.d}$	Integral sliding mode surfaces
sig(.)	Sigmoid function
$\dot{\hat{\theta}}_i$	Adaptive law

I.Introduction

The traction system is the core part of urban rail transit (URT). In recent years, permanent magnet synchronous motor (PMSM) with the advantages of high torque and power density, low maintenance and low torque ripple, has become the development direction of the next generation of traction motor in URT [1,3]. Among many modes of PMSM based URT, each train carriage contains multiple PMSMs (multi-PMSMs), and there is no mechanical connection between rotors of each PMSM. In the process of train operation, the linear speed of all wheels must be consistent. However, the working conditions of each wheel and traction motor may be different, and the friction between wheel and rail changes unsteadily due to the different load of each carriage. All these factors may cause idling and slipping of wheel pairs. Therefore, the speed synchronous cooperative performance between multiple traction motors in URT is of great significance.

Some cooperative control schemes have been studied and reported to realize cooperative control of multiple motors. In [4], a parallel structure was used to realize the cooperative control of multiple motors. Therein, there was no coupling relationship between the motors, thus if the load of one motor is disturbed, the synchronization accuracy cannot be guaranteed. In [5], the master-slave structure was proposed to improved the synchronization performance. However, it had no feedback link from the slave motor to the master motor [6]. Moreover, another disadvantage was losing the speed synchronization performance when the load torque changed. Meanwhile, the disturbance in the master motor would be transmitted to the slave motor, and the disturbance applied to the slave motor would not affect the master motor or other connected slave motors. The cross-coupling structure was adopted in the dual motor system to achieve accurate tracking performance [7]. The structure has strong anti-disturbance ability, but it is not suitable for the systems with more than two motors [8]. In [9], a relative coupling control was designed to realize the speed coupling between motors. Each motor adopted the speed synchronization compensator to ensure the synchronization performance of the system. However, the disadvantage of relative coupling control is that the speed compensation model will become more complicated with an increase in the number of motors. In conclusion, a appropriate cooperative control scheme is is urgently needed to guarantee the synchronization performance of multiple motors.

In recent years, multi-agent system (MAS) based cooperative control has become a hot topic in the control field. Generally, a single agent is regarded as a node, and the information interaction between agents is regarded as an edge [10]. At this time, the graph theory can be used to analyze the relationship between agents. In order to meet the consistency of multi-agent system, a leader agent with reference trajectory should be defined. Other agents called followers track leader's trajectory to achieve consistent tracking [11]. Recently, MAS has been widely used in unmanned aerial vehicle, spacecraft, mobile robot and other fields. In [12, 13], for a class of linear and nonlinear MAS, each agent was controlled by a distributed proportion-integral-differential (PID) controller and the tracking error of each agent can be converged to zero. However, the traditional PID speed controller was unable to meet the requirements of overshoot and fast response at the same time. Therefore, for the MAS, some advanced control strategies was adopted, such as fuzzy control, sliding mode control, backstepping control, etc [14]. In [15], an attempt was made on multiple induction motors, and multi-agent technology was applied to achieve the goal of speed synchronization. In [10], in order to solve the speed cooperative control problem of traction system driven by multiple linear induction motors, the multi-agent technology was introduced. However, in the field of cooperative control of multi-PMSMs, there is no relevant literature on the use of multi-agent technology. In this paper, each PMSM in URT is treated as an agent, and multi-PMSMs can be regarded as the MAS. The agent can communicate with other agents via the established directed-graph to achieve cooperative control.

On the other hand, during the operation of URT, the change of carriage load and the difference of railway conditions will cause load disturbances, and the overload or underload of motors will affect

the accuracy of cooperative control. To improve the anti-disturbance performance of the URT, an effective method is to provide the estimated the load information to the controller in real-time [16]. Therefore, the disturbance-observer (DO) has been proposed, especially sliding mode disturbance observer (SMDO) has the advantages of insensitivity to system parameter changes, which has been widely studied by the academic community. An extended SMDO was proposed in [17] and an adaptive reaching law was introduced, which verifies that the reaching law had advantages in suppressing chattering. In addition, the SMDO in [18] used the nonlinear approaching law to solve the approaching time and chattering problems. However, none of the above extended SMDO can guarantee that the perturbation observation error converges in finite-time. In [19], a finite-time DO was proposed. Nevertheless, this structure of DO has many parameters and needs to be designed reasonably, which is not conducive to engineering application. Moreover, compared with traditional first-order SMDO, high-order SMDO has better performance in chattering suppression [20]. Therefore, an super-twisting algorithm (STA) based finite-time DO is designed in this paper to realize fast and accurate estimation of disturbance.

Motivated by the analysis of previous research results, and combined with the characteristics of the multi-PMSMs traction system in low-speed URT, a finite-time disturbance-observer-based fuzzy sliding mode cooperative backstepping (FDFSM-CB) scheme is designed to reduce the synchronization error under disturbance. Compared with the existing results, the main contributions are as follows:

1) The multi-PMSMs system is considered as a MAS, and the neighborhood synchronization errors are defined to describe the mode of information transmission between neighboring PMSMs via directed-graph theory.

2) A finite-time DO is proposed in this paper to estimate the load and disturbance torque of PMSMs, which reduces the influence of disturbance and improves the speed synchronization accuracy in actual operation.

3) The fuzzy logic systems (FLSs) are utilized to approximate the uncertain and nonlinear parts of the PMSM dynamic model, which improve the robustness of the controller under uncertain motor parameters.

This paper is structured as follows. In Section II, the dynamic model of PMSM is established, and some used lemmas are given. In Section III, the FDFSM-CB scheme is designed based on the directed-graph, and the finite-time stability of the system is proved. In Section IV, the hardware-in-the-loop (HIL) results are given and analyzed. In Section V, the conclusions are summarized.

II.Problem Formulation and Preliminaries

A.Dynamic Model of multi-PMSMs

The structure of a low-speed URT System is shown in Fig. 1. The train of URT obtains electricity from the DC catenary through the pantograph. The URT train contains several PMSMs. There is no mechanical connection between rotors of each PMSM, and one PMSM must be driven by one inverter module. In Fig. 2, the DC power is converted into AC power by the traction inverter and transmitted to the PMSM. Then, the motor speed is controlled by a traction control unit. In addition, each PMSM is regarded as an agent, and the signals transmitted between adjacent PMSMs are realized through a communication module. Thus, the multi-PMSMs can be regarded as the MAS.

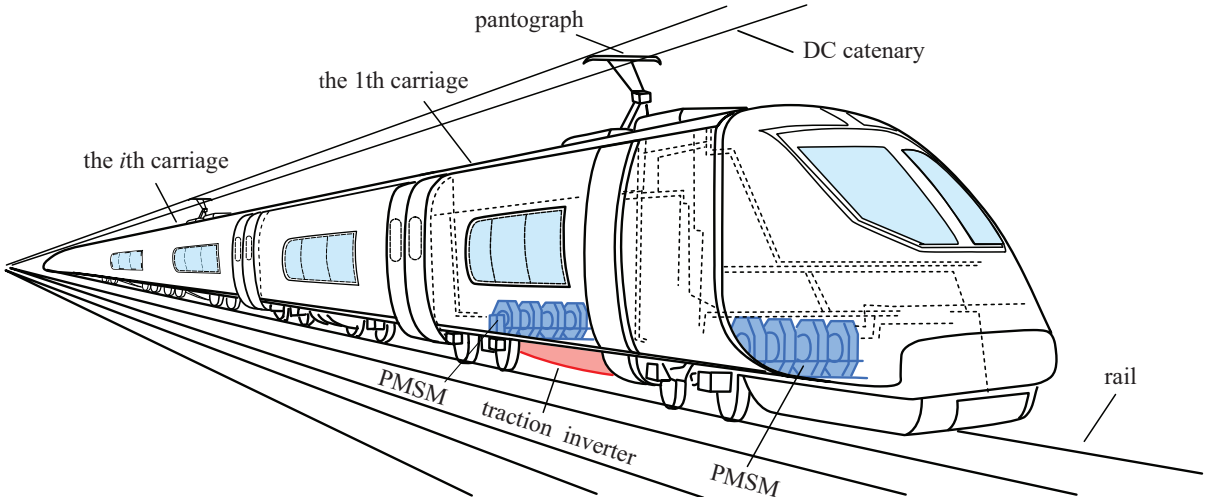

Figure 1: Structure of low-speed URT Systems.

In low-speed URT, due to the short distance between stations, trains need to switch frequently between startup, acceleration, deceleration and braking states. Therefore, traction motors need to have good performance in the medium and low speed range. In this paper, the non-salient pole PMSM is selected as the traction motor of low-speed URT, and the dynamic model of the i th ($i = 1, 2, ..., n$) non-salient pole PMSM in d-q frame is expressed as follows [21],

$$\begin{aligned}
\frac{di_{i.d}}{dt} &= -\frac{R_s}{L_s} i_{i.d} + p\omega_{i.g} i_{i.q} + \frac{1}{L_s} u_{i.d} \\
\frac{di_{i.q}}{dt} &= -\frac{R_s}{L_s} i_{i.q} - p\omega_{i.g} i_{i.d} - p\omega_{i.g} \frac{\varphi_f}{L_s} + \frac{1}{L_s} u_{i.q} \\
T_{i.m} &= \frac{3}{2} p\varphi_f i_{i.q}
\end{aligned} \tag{1}$$

where $i_{i.d}$, $i_{i.q}$ are d-q axis stator current of the i th PMSM, $u_{i.d}$, $u_{i.q}$ are d-q axis control voltage of the i th PMSM, p is the number of pole pairs, R_s represents the armature resistance, φ_f denotes the permanent magnet flux, L_s denotes the stator inductance, and $T_{i.m}$ is electromagnetic torque of the i th PMSM.

Besides, the mechanical dynamics of the i th PMSM can be expressed as

$$\frac{d\omega_{i.g}}{dt} = \frac{1}{J}\left(T_{i.m} - F\omega_{i.g} - T_{i.L} - T_{i.d}\right) \tag{2}$$

where F denotes the rotor viscous friction, J represents the equivalent inertia, $\omega_{i.g}$ denotes the i th rotor angular speed, $T_{i.L}$ and $T_{i.d}$ represent load and disturbance torques of i th motor, and $T_{i.\delta} = T_{i.d} + T_{i.L}$. Define $[x_{i.1}, x_{i.2}, x_{i.3}]^T = [\omega_{i.g}, i_{i.q}, i_{i.d}]^T$, $\phi_{i.\delta} = -(T_{i.\delta})/J$, (1) and (2) can be rewritten as

$$\begin{aligned}
\dot{x}_{i.1} &= \frac{1}{J}\left(\frac{3}{2}p\varphi_f x_{i.2} - Fx_{i.1}\right) + \phi_{i.\delta} \\
\dot{x}_{i.2} &= -\frac{R_s}{L_s}x_{i.2} - px_{i.1}x_{i.3} - px_{i.1}\frac{\varphi_f}{L_s} + \frac{1}{L_s}u_{i.q} \\
\dot{x}_{i.3} &= -\frac{R_s}{L_s}x_{i.3} + px_{i.1}x_{i.2} + \frac{1}{L_s}u_{i.d}
\end{aligned} \tag{3}$$

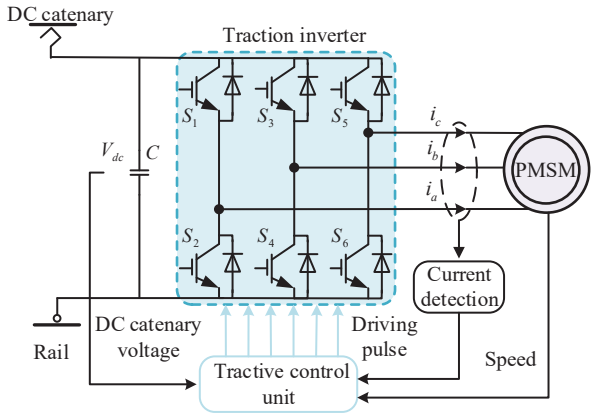

Figure 2: The circuit structure of ith PMSM in URT.

B.Directed-Graph Theory

The directed-graph $G = (\mathscr{V}, \mathscr{Y}, A)$ describes the communication direction of MAS [10,22,23]. Therein, $\mathscr{V} = \{\nu_1, \nu_2, ..., \nu_n\}$ denotes the set of nodes, and $\mathscr{Y} \subseteq \mathscr{V} \times \mathscr{V}$ indicates the set of edges. The edge (v_i, v_j) represents the communication direction form the node i to node j. The adjacency matrix $A = [a_{ij}]_{n\times n}$ is used to indicate the information transmission direction between agents. If $(v_j, v_i) \in \mathscr{Y}$, then $a_{ij} = 1$, otherwise $a_{ij} = 0$, and $a_{ii} = 0$ is always holds. Moreover, the Laplacian matrix is established as $L = [l_{ij}]_{n\times n} = D - A$, and $D = diag\,(d_1, d_2, ..., d_n)$ with $d_i = \sum_{j=1}^{n} a_{ij}$. To represent the communication between each follower and leader, define the diagonal matrix $B = diag\,(b_1, b_2, ..., b_n)$, and if the follower node i can get information form the leader node, $b_i = 1$, otherwise $b_i = 0$.

C.Some Lemmas

To design the FDFSM-CB scheme and stability analysis, the following Lemmas are introduced.

Lemma 1 [24]: For a compact set Δ, if a continuous function $\ell(x)$ is delimited on Δ, there has the FLS $W^T\partial(x)$ such that

$$\sup_{x\in\Delta}\left|\ell(x)-W^T\partial(x)\right|\leq\varsigma \tag{4}$$

where ς is any positive constant, $W=[W_1,...,W_N]^T\in \mathrm{R}^N$ represents the weight vector, and $\partial(x)=[\kappa_1(x),\kappa_2(x),...,\kappa_N(x)]^T/\sum_{i=1}^{N}\kappa_i(x)$ is the basis function vector. $\kappa_i(x)$ is the Gaussian function expressed as $\kappa_i(x)=\exp\left[\left(-(x-o_i)^T(x-o_i)\right)\Big/\varpi_i^2\right]$, ϖ_i is the width, and $o_i=[o_{i1},o_{i2},...,o_{in}]^T$ is the center vector.

Lemma 2 [25]: For positive scalar $\iota>1/2$, there has the inequality $-\tilde{a}\hat{a}\leq[(-(2\iota-1))/2\iota]\,\tilde{a}^2+(\iota/2)\,a^2$, where $\tilde{a}=\hat{a}-a$.

Lemma 3 [26]: For $x_i\in R$, $i=1,2,...,n$, $0<q\leq 1$.

$$\left(\sum_{i=1}^{n}|x_i|\right)^q\leq\sum_{i=1}^{n}|x_i|^q\leq n^{1-q}\left(\sum_{i=1}^{n}|x_i|\right)^q \tag{5}$$

Lemma 4 [27]: The standard STA with a disturbance term can be expressed as

$$\begin{aligned}\dot{\vartheta}_1&=-g_1|\vartheta_1|^{1/2}\mathrm{sign}(\vartheta_1)+\vartheta_2\\ \dot{\vartheta}_2&=-g_2\mathrm{sign}(\vartheta_1)+\dot{\chi}(t)\end{aligned} \tag{6}$$

where ϑ_1 and ϑ_2 are the state variables, g_1 and g_2 are designed positive gains, sign(.) represents the symbolic function, $\chi(t)$ is the continuously differentiable and bounded disturbance term, and $\|\dot{\chi}(t)\|\leq\gamma$. If the gains of (6) meet the condition

$$M^TP+PM+\gamma^2C^TC+PHH^TP=-Q<0 \tag{7}$$

where P and Q are positive and symmetric definite matrixs, $M=\begin{bmatrix}-1/2g_1 & 1/2\\ -g_2 & 0\end{bmatrix}$, $H=\begin{bmatrix}0\\1\end{bmatrix}$, $C=\begin{bmatrix}1 & 0\end{bmatrix}$, all trajectories of the system (6) can be converged in finite-time. Besides, the quadratic form $V(\vartheta)=\zeta^TP\zeta$ is the Lyapunov function for the system (6), and $\zeta^T=\left[|\vartheta_1|^{1/2}\mathrm{sign}(\vartheta_1),\vartheta_2\right]$. The trajectory reaches the origin in a time smaller than

$$T_d=\frac{2}{\mathscr{K}(P)}V^{1/2}(\vartheta_0),\ \mathscr{K}(P)\triangleq\frac{\lambda_{\min}(Q)\,\lambda_{\min}^{1/2}(P)}{\lambda_{\max}(P)} \tag{8}$$

where $\lambda_{\min}\{\cdot\}$ and $\lambda_{\max}\{\cdot\}$ are defined as the minimum and maximum eigenvalues of the matrix, ϑ_0 is the initial state.

III.Design of the FDFSM-CB Scheme and Stability Analysis

In this section, based on the directed-graph, the FDFSM-CB scheme is designed for multi-PMSMs. The subscript i $(i=1,2,...,n)$ represents the label of the i th PMSM. The controllers are completely

distributed and interact with each other through the established communication topology, the control goal is to track the speed of multi-PMSMs cooperatively. Throughout the controller design process, define estimation error $\tilde{*}=\hat{*}-*$, where $\hat{*}$ is the estimation for the variable $*$. Based the proposed distributed FDFSM-CB control scheme, the control structure of each PMSM controller is the same, which is shown in Fig. 3.

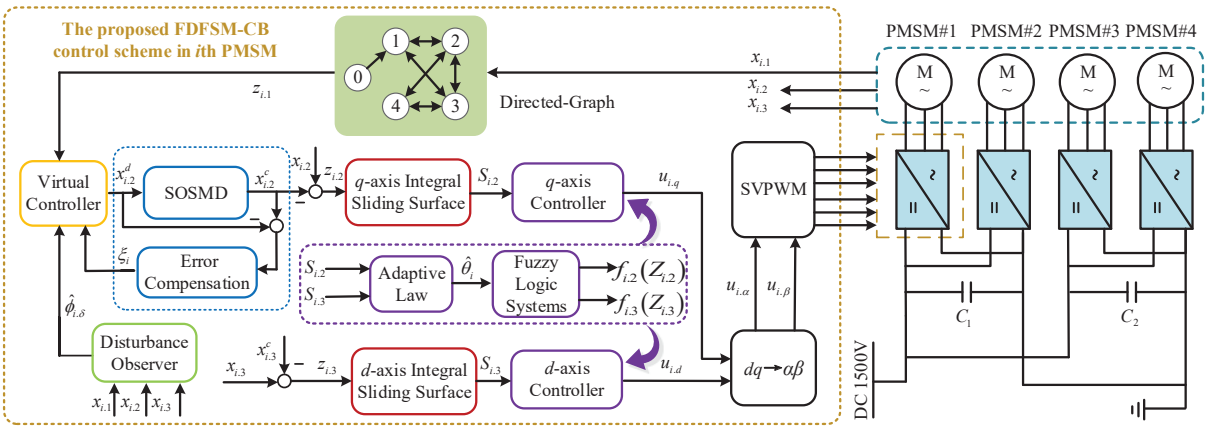

Figure 3: Control diagram of proposed FDFSM-CB control scheme.

A.Disturbance-Observer Design

To facilitate the design of DO, the state equation of the system (3) should be rewritten as

$$\dot{x} = f(x) + gu + \phi(t) \tag{9}$$

where

$$\begin{aligned} &x = [x_{i.1}, x_{i.2}, x_{i.3}]^T, u = [u_{i.d}, u_{i.q}]^T, \\ &f(x) = \begin{bmatrix} \left(\frac{3}{2}p\varphi_f x_{i.2} - Fx_{i.1}\right)/J \\ -\frac{R_s x_{i.2}}{L_s} - px_{i.1}x_{i.3} - \frac{p\varphi_f x_{i.1}}{L_s} \\ -\frac{R_s}{L_s}x_{i.3} + px_{i.1}x_{i.2} \end{bmatrix}, \\ &g = \begin{bmatrix} 0 & \frac{1}{L_s} & 0 \\ 0 & 0 & \frac{1}{L_s} \end{bmatrix}^T, \phi = [\phi_{i.\delta}, 0, 0]^T \end{aligned} \tag{10}$$

Then, assume $\left\|\dot{\phi}(t)\right\| \leq \gamma_d$, the finite-time DO is designed as

$$\begin{aligned} \dot{\hat{x}} &= f(x) + gu - \alpha_{i.1d}\mathrm{sgn}^{1/2}(\hat{x} - x) + \hat{\phi} \\ \dot{\hat{\phi}} &= -\alpha_{i.2d}\mathrm{sgn}^0(\hat{x} - x) \end{aligned} \tag{11}$$

where $\alpha_{i.1d}$ and $\alpha_{i.2d}$ are the positive observer gains, $\mathrm{sgn}^b(\hat{x} - x) = \left[\mathrm{sgn}^b(\tilde{x}_1), \mathrm{sgn}^b(\tilde{x}_2), \mathrm{sgn}^b(\tilde{x}_3)\right]^T$, and $\mathrm{sgn}^b(\tilde{x}_i) = |\tilde{x}_i|^b \mathrm{sign}(\tilde{x}_i)$, $i = 1, 2, 3$. The finite-time convergence of DO (11) is given by the following corollary.

Corollary 1: Consider the system (9) with disturbances, the DO (11) is applied and the appropriate parameters are selected, the disturbance observation error vector $z_d = \hat{\phi} - \phi$ can be converged in finite-time.

Proof: According to (9) and (11), the error dynamics are defined as

$$\begin{aligned} \dot{\tilde{x}} &= -\alpha_{i.1d}\mathrm{sgn}^{1/2}(\tilde{x}) + z_d \\ \dot{z}_d &= -\alpha_{i.2d}\mathrm{sgn}^{0}(\tilde{x}) - \dot{\phi} \end{aligned} \tag{12}$$

Considering the condition $\left\|\dot{\phi}(t)\right\| \leq \gamma_d$ and Lemma 4, the observer error z_d can be converged in finite-time.

Remark 1: The greater the observer gains $\alpha_{i.1d}$ and $\alpha_{i.2d}$ of DO (11), the faster convergence of observation error. But too large gains may cause violent chattering. Thus, the selection of DO parameters is a trade-off process, which needs to obtain the best value through repeated tests.

B.Construct the virtual control law and compensated tracking error

The angular speed tracking error of the i th PMSM is defined as

$$e_{i.1} = x_{i.1} - x_1^c \tag{13}$$

where x_1^c is the desired angular speed of multi-PMSMs.

To describe the information interaction state between distributed controllers, based on directed-graph theory in Section II-B, the neighborhood synchronization error $z_{i.1}$ for i th agent is defined as

$$\begin{aligned} z_{i.1} &= \sum_{j=1}^{n} a_{ij}\left(e_{i.1} - e_{j.1}\right) + b_i e_{i.1} \\ &= \sum_{j=1}^{n} a_{ij}\left(x_{i.1} - x_{j.1}\right) + b_i\left(x_{i.1} - x_1^c\right) \end{aligned} \tag{14}$$

Then, construct Lyapunov function as

$$V_{i.1} = \frac{1}{2} z_{i.1}^2 \tag{15}$$

Combining (3) and (14), the derivative of $V_{i.1}$ is calculated as

$$\begin{aligned} \dot{V}_{i.1} &= z_{i.1}\left[\sum_{j=1}^{n} a_{ij}\left(\dot{x}_{i.1} - \dot{x}_{j.1}\right) + b_i\left(\dot{x}_{i.1} - \dot{x}_1^c\right)\right] \\ &= -k_{i.1} z_{i.1}^2 + z_{i.1}\left[k_{i.1} z_{i.1} - \sum_{j=1}^{n} a_{ij}\dot{x}_{j.1} - b_i \dot{x}_1^c + \right. \\ &\quad \left. (d_i + b_i)\left(\frac{3p\varphi_f}{2J} x_{i.2} - \frac{F}{J} x_{i.1} + \phi_{i.\delta}\right)\right] \end{aligned} \tag{16}$$

Based on (16), choose a virtual control law $x_{i.2}^d$ for i th PMSM as follows

$$\begin{aligned} x_{i.2}^d = \frac{2}{3p\varphi_f\left(d_i+b_i\right)}\Big[&\left(d_i+b_i\right)Fx_{i.1} - Jk_{i.1}z_{i.1} \\ &+ Jb_i\dot{x}_1^c - J\left(d_i+b_i\right)\hat{\phi}_{i.\delta} + J\sum_{j=1}^{n} a_{ij}\dot{x}_{j.1} - Jc_{i.1}\bar{z}_{i.1}^{\beta}\Big] \end{aligned} \tag{17}$$

where $k_{i.1}$, $c_{i.1}$, β are positive constants, and $0<\beta<1$. $\bar{z}_{i.1}$ is defined in (20).

The second-order sliding mode differentiator (SOSMD) is designed to estimate the derivative of the virtual control law in finite-time, which reduces the noise caused by the direct derivation of (17). The SOSMD is designed as

$$\begin{aligned} \dot{\psi}_{i.1} &= \eta_{i.1} \\ \eta_{i.1} &= -\Upsilon_{i.1}|\psi_{i.1}-\varsigma_{i.r}|^{1/2}\mathrm{sign}\left(\psi_{i.1}-\varsigma_{i.r}\right)+\psi_{i.2} \\ \dot{\psi}_{i.2} &= -\Upsilon_{i.2}\mathrm{sign}\left(\psi_{i.2}-\eta_{i.1}\right) \end{aligned} \tag{18}$$

where $\Upsilon_{i.1}$ and $\Upsilon_{i.2}$ are positive gains, $\varsigma_{i.r}$ is the input signal of SOSMD, $\psi_{i.1}=x_{i.2}^c$ and $\eta_{i.1}=\dot{x}_{i.2}^c$ are the estimations for the $\varsigma_{i.r}$ and $\dot{\varsigma}_{i.r}$.

Remark 2 [28]: By adjusting the gains of $\Upsilon_{i.1}$ and $\Upsilon_{i.2}$, the derivative of the input signal can be estimated within finite-time. Besides, the gains $\Upsilon_{i.1}$ and $\Upsilon_{i.2}$ should be large enough.

The error compensating signals ξ_i is defined as

$$\dot{\xi}_i = -k_{i.1}\xi_i + \frac{3p\varphi_f\left(d_i+b_i\right)}{2J}\left(x_{i.2}^c - x_{i.2}^d\right) - l_i\mathrm{sign}\left(\xi_i\right) \tag{19}$$

where $l_i>0$ is a designed constant.

Then, the compensated tracking error is defined as

$$\bar{z}_{i.1} = z_{i.1} - \xi_i \tag{20}$$

C.Construct the real control law and adaptive law

The current tracking errors of i th PMSM are defined as

$$z_{i.2} = x_{i.2} - x_{i.2}^c, \quad z_{i.3} = x_{i.3} - x_{i.3}^c \tag{21}$$

where $x_{i.2}^c$ and $x_{i.3}^c=0$ represent the reference values of q-axis and d-axis currents.

According to (3), (17), (19) and (21) the derivative of (20) can be calculated as

$$\begin{aligned} \dot{\bar{z}}_{i.1} = \dot{z}_{i.1} - \dot{\xi}_i = &\frac{3p\varphi_f\left(d_i+b_i\right)}{2J}z_{i.2} - k_{i.1}\bar{z}_{i.1} \\ &- \left(d_i+b_i\right)\tilde{\phi}_{i.\delta} + l_i\mathrm{sign}\left(\xi_i\right) - c_{i.1}\bar{z}_{i.1}^{\beta} \end{aligned} \tag{22}$$

To stabilize error $\bar{z}_{i.1}$, the Lyapunov function is chosen as $V_{i.2} = \bar{z}_{i.1}^2/2$, and then the derivative of $V_{i.2}$ is calculated as

$$\begin{aligned}\dot{V}_{i.2} = \bar{z}_{i.1}\Bigg[&-k_{i.1}\bar{z}_{i.1} + \frac{3p\varphi_f\left(d_i + b_i\right)}{2J}z_{i.2} \\ &- \left(d_i + b_i\right)\tilde{\phi}_{i.\delta} + l_i\text{sign}\left(\xi_i\right) - c_{i.1}\bar{z}_{i.1}^{\beta}\Bigg]\end{aligned} \tag{23}$$

Define the integral sliding mode surface

$$\begin{aligned}S_{i.q} = S_{i.2} &= z_{i.2} + \mu_{i.2}\int_0^t z_{i.2}\left(\sigma\right)d\sigma \\ S_{i.d} = S_{i.3} &= z_{i.3} + \mu_{i.3}\int_0^t z_{i.3}\left(\sigma\right)d\sigma\end{aligned} \tag{24}$$

where $\mu_{i.2}$ and $\mu_{i.3}$ are positive gains. Then, the sliding mode reaching law is defined as

$$\begin{aligned}\dot{S}_{i.2} &= -h_{i.2}\text{sig}\left(S_{i.2}\right) - \rho_{i.2}S_2 \\ \dot{S}_{i.3} &= -h_{i.3}\text{sig}\left(S_{i.3}\right) - \rho_{i.3}S_3\end{aligned} \tag{25}$$

where $h_{i.2}$, $h_{i.3}$, $\rho_{i.2}$ and $\rho_{i.3}$ are positive constants. The Sigmoid function sig(.) is used to reduce the chattering of symbolic function, which is defined as

$$\text{sig}\left(x\right) = \frac{2}{1 + \exp\left(-\mathscr{Q}x\right)} - 1 \tag{26}$$

where the positive constant $\mathscr{Q}$ represents the convergence rate.

Based on (3), the derivation of (24) can be obtained

$$\begin{aligned}\dot{S}_{i.2} = \dot{z}_{i.2} + \mu_{i.2}z_{i.2} = &-\frac{R_s}{L_s}x_{i.2} - px_{i.1}x_{i.3} - \\ &px_{i.1}\frac{\varphi_f}{L_s} + \frac{1}{L_s}u_{i.q} - \dot{x}_{i.2}^c + \mu_{i.2}z_{i.2}\end{aligned} \tag{27}$$

$$\begin{aligned}\dot{S}_{i.3} = \dot{z}_{i.3} + \mu_{i.3}z_{i.3} = &-\frac{R_s}{L_s}x_{i.3} + px_{i.1}x_{i.2} + \\ &\frac{1}{L_s}u_{i.d} + \mu_{i.3}z_{i.3}\end{aligned} \tag{28}$$

Then, construct Lyapunov function as

$$V_{i.3} = V_{i.2} + \frac{1}{2}S_{i.2}^2 \tag{29}$$

According to (27), the derivative of (29) can be obtained

$$\begin{aligned}\dot{V}_{i.3} = \dot{V}_{i.2} - h_{i.2}S_{i.2}\text{sig}\left(S_{i.2}\right) - \rho_{i.2}S_{i.2}^2 + S_{i.2}\Bigg(&f_{i.2}\left(Z_{i.2}\right) \\ &+ \frac{1}{L_s}u_{i.q} - \dot{x}_{i.2}^c + \mu_{i.2}z_{i.2} + h_{i.2}\text{sig}\left(S_{i.2}\right) + \rho_{i.2}S_{i.2}\Bigg)\end{aligned} \tag{30}$$

where $f_{i.2}\left(Z_{i.2}\right) = -\frac{R_s}{L_s}x_{i.2} - px_{i.1}x_{i.3} - px_{i.1}\frac{\varphi_f}{L_s}$, $Z_{i.2} = \left[x_{i.1}, x_{i.2}, x_{i.3}\right]^T$. Following the Lemma 1, for $f_{i.2}\left(Z_{i.2}\right)$, there is an FLS $W_{i.2}^T\partial_{i.2}\left(Z_{i.2}\right)$ that satisfies

$$f_{i.2}\left(Z_{i.2}\right) = W_{i.2}^T\partial_{i.2}\left(Z_{i.2}\right) + \wp_{i.2}\left(Z_{i.2}\right) \tag{31}$$

where $\wp_{i.2}(Z_{i.2})$ denotes the FLS approximation error and $|\wp_{i.2}(Z_{i.2})| \leq \upsilon_{i.2}$. According to Young's inequality, we have

$$\begin{aligned} S_{i.2}f_{i.2} \leq \frac{1}{2\lambda_{i.2}^2}S_{i.2}^2\|W_{i.2}\|^2\partial_{i.2}^T\partial_{i.2}+ \\ \frac{1}{2}\lambda_{i.2}^2+\frac{1}{2}S_{i.2}^2+\frac{1}{2}\upsilon_{i.2}^2 \end{aligned} \tag{32}$$

where $\lambda_{i.2}$ is the positive constant, $\|W_{i.2}\|$ is the norm of $W_{i.2}$.

Substituting (32) into (30), one has

$$\begin{aligned} \dot{V}_{i.3} \leq \dot{V}_{i.2}+\Bigg[S_{i.2}\Bigg(\frac{1}{2\lambda_{i.2}^2}S_{i.2}\|W_{i.2}\|^2\partial_{i.2}^T\partial_{i.2}+\frac{1}{2}S_{i.2}+ \\ h_{i.2}\mathrm{sig}(S_{i.2})+\rho_{i.2}S_{i.2}+\mu_{i.2}z_{i.2}-\dot{x}_{i.2}^c+\frac{1}{L_s}u_{i.q}\Bigg)\Bigg] \\ -h_{i.2}S_{i.2}\mathrm{sig}(S_{i.2})-\rho_{i.2}S_{i.2}^2+\frac{1}{2}\lambda_{i.2}^2+\frac{1}{2}\upsilon_{i.2}^2 \end{aligned} \tag{33}$$

Then, design the real control law $u_{i.q}$ for i th PMSM as

$$\begin{aligned} u_{i.q}=L_s\Bigg[-\rho_{i.2}S_{i.2}-h_{i.2}\mathrm{sig}(S_{i.2})-\frac{1}{2}S_{i.2}- \\ \frac{1}{2\lambda_{i.2}^2}S_{i.2}\hat{\theta}_i\partial_{i.2}^T\partial_{i.2}+\dot{x}_{i.2}^c-\mu_{i.2}z_{i.2}-c_{i.2}S_{i.2}^{\beta}\Bigg] \end{aligned} \tag{34}$$

where $\hat{\theta}_i$ is the estimation for the θ_i, which will be determined later. Substituting (34) into (33) gives

$$\begin{aligned} \dot{V}_{i.3} \leq \dot{V}_{i.2}-h_{i.2}S_{i.2}\mathrm{sig}(S_{i.2})-\rho_{i.2}S_{i.2}^2-c_{i.2}S_{i.2}^{\beta+1}+ \\ \frac{1}{2\lambda_{i.2}^2}S_{i.2}^2\left(\|W_{i.2}\|^2-\hat{\theta}_i\right)\partial_{i.2}^T\partial_{i.2}+\frac{1}{2}\lambda_{i.2}^2+\frac{1}{2}\upsilon_{i.2}^2=\mathscr{R} \end{aligned} \tag{35}$$

Further, to construct the controller $u_{i.d}$, select the Lyapunov function is

$$V_{i.4}=V_{i.3}+\frac{1}{2}S_{i.3}^2 \tag{36}$$

According to (28), the derivative of $V_{i.4}$ can be calculated as

$$\begin{aligned} \dot{V}_{i.4} \leq \mathscr{R}+S_{i.3}\Bigg(h_{i.3}\mathrm{sig}(S_{i.3})+\mu_{i.3}z_{i.3}+f_{i.3}(Z_{i.3}) \\ +\frac{1}{L_s}u_{i.q}+\rho_{i.3}S_{i.3}\Bigg)-h_{i.3}S_{i.3}\mathrm{sig}(S_{i.3})-\rho_{i.3}S_{i.3}^2 \end{aligned} \tag{37}$$

where $f_{i.3}(Z_{i.3})=-\frac{R_s}{L_s}x_{i.3}+px_{i.1}x_{i.2}$, $Z_{i.3}$=$Z_{i.2}$. Similar to (31), based on Lemma 1, $f_{i.3}(Z_{i.3})$ can be approximated by an FLS $W_{i.3}^T\partial_{i.3}(Z_{i.3})$. For given $\upsilon_{i.3}>0$, one obtains

$$\begin{aligned} S_{i.3}f_{i.3} \leq \frac{1}{2\lambda_{i.3}^2}S_{i.3}^2\|W_{i.3}\|^2\partial_{i.3}^T\partial_{i.3}+ \\ \frac{1}{2}\lambda_{i.3}^2+\frac{1}{2}S_{i.3}^2+\frac{1}{2}\upsilon_{i.3}^2 \end{aligned} \tag{38}$$

where constant $\lambda_{i.3}>0$, $\|W_{i.3}\|$ is the norm of $W_{i.3}$.

Combining (38), (37) can be rewritten as

$$\begin{aligned}\dot{V}_{i.4} \leq & \left[S_{i.3}\left(\frac{1}{2\lambda_{i.3}^2}S_{i.3}\|W_{i.3}\|^2\partial_{i.3}^T\partial_{i.3}+\frac{1}{2}S_{i.3}+\right.\right.\\ & \left.\left.h_{i.3}\mathrm{sig}\left(S_{i.3}\right)+\rho_{i.2}S_{i.3}+\mu_{i.3}z_{i.3}+\frac{1}{L_s}u_{i.d}\right)\right]\\ & -h_{i.3}S_{i.3}\mathrm{sig}\left(S_{i.3}\right)-\rho_{i.3}S_{i.3}^2+\frac{1}{2}\lambda_{i.3}^2+\frac{1}{2}\upsilon_{i.3}^2+\mathscr{R}\end{aligned} \tag{39}$$

Then, the real control law of i th PMSM $u_{i.d}$ is designed as

$$\begin{aligned}u_{i.d}=L_s\left[\right. & -\rho_{i.3}S_{i.3}-h_{i.3}\mathrm{sig}\left(S_{i.3}\right)-\frac{1}{2}S_{i.3}-\\ & \left.\frac{1}{2\lambda_{i.3}^2}S_{i.3}\hat{\theta}_i\partial_{i.3}^T\partial_{i.3}-\mu_{i.3}z_{i.3}-c_{i.3}S_{i.3}^{\beta}\right]\end{aligned} \tag{40}$$

Define $\theta_i=\max\left\{\|W_{i.2}\|^2,\|W_{i.3}\|^2\right\}$. Combining (16), (39) and (40), we have

$$\begin{aligned}\dot{V}_{i.4} \leq & -k_{i.1}\bar{z}_{i.1}^2+\sum_{m=2}^{3}\left(\frac{1}{2}\lambda_{i.m}^2+\frac{1}{2}\upsilon_{i.m}^2\right)-c_{i.1}\bar{z}_{i.1}^{\beta+1}\\ & +\sum_{m=2}^{3}\frac{1}{2\lambda_{i.m}^2}S_{i.m}^2\partial_{i.m}^T\partial_{i.m}\left(\theta_i-\hat{\theta}_i\right)-\sum_{m=2}^{3}c_{i.m}S_{i.m}^{\beta+1}\\ & +\bar{z}_{i.1}l_i\mathrm{sign}\left(\xi_i\right)-\bar{z}_{i.1}\tilde{\phi}_{i.\delta}(d_i+b_i)+\frac{3p\varphi_f\left(d_i+b_i\right)\bar{z}_{i.1}z_{i.2}}{2J}\\ & -\sum_{m=2}^{3}\left[h_{i.m}S_{i.m}\mathrm{sig}\left(S_{i.m}\right)+\rho_{i.m}S_{i.m}^2\right]\end{aligned} \tag{41}$$

To choose the adaptive law $\hat{\theta}_i$, we construct the Lyapunov function as

$$V_{i.5}=V_{i.4}+\frac{\tilde{\theta}_i^2}{2r_i} \tag{42}$$

where $r_i>0$.

Then, the derivative of (42) can be obtained

$$\begin{aligned}\dot{V}_{i.5} \leq & -k_{i.1}\bar{z}_{i.1}^2-c_{i.1}\bar{z}_{i.1}^{\beta+1}+\sum_{m=2}^{3}\left(\frac{1}{2}\lambda_{i.m}^2+\frac{1}{2}\upsilon_{i.m}^2\right)\\ & -\bar{z}_{i.1}\tilde{\phi}_{i.\delta}(d_i+b_i)+\bar{z}_{i.1}z_{i.2}\frac{3p\varphi_f\left(d_i+b_i\right)}{2J}-\sum_{m=2}^{3}c_{i.m}S_{i.m}^{\beta+1}\\ & +\bar{z}_{i.1}l_i\mathrm{sign}\left(\xi_i\right)+\frac{\tilde{\theta}_i}{r_i}\left[\dot{\hat{\theta}}_i-\sum_{m=2}^{3}\frac{r_i}{2\lambda_{i.m}^2}S_{i.m}^2\partial_{i.m}^T\partial_{i.m}\right]\\ & -\sum_{m=2}^{3}\left[h_{i.m}S_{i.m}\mathrm{sig}\left(S_{i.m}\right)+\rho_{i.m}S_{i.m}^2\right]\end{aligned} \tag{43}$$

Thus, the adaptive law of i th PMSM is designed as

$$\dot{\hat{\theta}}_i=\sum_{m=2}^{3}\frac{r_i}{2\lambda_{i.m}^2}S_{i.m}^2\partial_{i.m}^T\partial_{i.m}-2r_i\varepsilon_i\hat{\theta}_i \tag{44}$$

where $\lambda_{i.m}$, r_i, ε_i are positive constants.

D.Stability analysis

Construct the Lyapunov function

$$V = \sum_{i=1}^{n} V_{i.4} + \frac{1}{2}\sum_{i=1}^{n}\frac{\tilde{\theta}_i^2}{r_i} \tag{45}$$

According to the properties of sig(.) function, we have $\sum_{m=2}^{3}\left[h_{i.m}S_{i.m}\mathrm{sig}\left(S_{i.m}\right)\right] \geq 0$. Then, combining (44), the derivative of (45) is calculated as

$$\begin{aligned}\dot{V} \leq & -\sum_{i=1}^{n} k_{i.1}\bar{z}_{i.1}^2 - \sum_{i=1}^{n}\sum_{m=2}^{3}\left(\rho_{i.m}S_{i.m}^2 + c_{i.m}S_{i.m}^{\beta+1}\right) \\ & + \sum_{i=1}^{n}\sum_{m=2}^{3}\left(\frac{1}{2}\lambda_{i.m}^2 + \frac{1}{2}\upsilon_{i.m}^2\right) + \sum_{i=1}^{n}\bar{z}_{i.1}z_{i.2}\frac{3p\varphi_f\left(d_i+b_i\right)}{2J} \\ & + \sum_{i=1}^{n}\left[\bar{z}_{i.1}l_i\mathrm{sign}\left(\xi_i\right) - 2\varepsilon_i\tilde{\theta}_i\hat{\theta}_i - \bar{z}_{i.1}\tilde{\phi}_{i.\delta}(d_i+b_i) - c_{i.1}\bar{z}_{i.1}^{\beta+1}\right]\end{aligned} \tag{46}$$

By using Young's inequality, we have

$$\begin{aligned}&\bar{z}_{i.1}l_i\mathrm{sign}\left(\xi_i\right) \leq \frac{l_i}{2}\bar{z}_{i.1}^2 + \frac{l_i}{2}[\mathrm{sign}\left(\xi_i\right)]^2 \leq \frac{l_i}{2}\bar{z}_{i.1}^2 + \frac{l_i}{2} \\ &-\left(d_i+b_i\right)\tilde{\phi}_{i.\delta} \leq o_{i.\delta}\end{aligned} \tag{47}$$

where $\tilde{\phi}_{i.\delta}$ is the observation error of DO. According to Corollary 1, the observation error $\tilde{\phi}_{i.\delta}$ converges to neighborhood $o_{i.\delta}$ in finite-time, i.e., $\left|\tilde{\phi}_{i.\delta}\right| \leq o_{i.\delta}$.

In addition, to eliminate the coupling term $\bar{z}_{i.1}z_{i.2}\frac{3p\varphi_f(d_i+b_i)}{2J}$, define $0 < \tau_i < 1$, one obtains

$$\begin{aligned}-k_{i.1}\bar{z}_{i.1}^2 + \bar{z}_{i.1}z_{i.2}\frac{3p\varphi_f\left(d_i+b_i\right)}{2J} &\leq -k_{i.1}\tau_i|\bar{z}_{i.1}|^2 \\ -k_{i.1}\left(1-\tau_i\right)\bar{z}_{i.1}^2 + \frac{3p\varphi_f\left(d_i+b_i\right)}{2J}\left|\bar{z}_{i.1}\right|\left|z_{i.2}\right|&\end{aligned} \tag{48}$$

Assuming $\frac{3p\varphi_f(d_i+b_i)}{2J}\left|\bar{z}_{i.1}\right|\left|z_{i.2}\right| - k_{i.1}\tau_i|\bar{z}_{i.1}|^2 \leq 0$, i.e., $|\bar{z}_{i.1}| \geq \frac{3p\varphi_f(d_i+b_i)|z_{i.2}|}{2k_{i.1}\tau_i J}$, the inequality (48) can be given as

$$-k_{i.1}\bar{z}_{i.1}^2 + \frac{3p\varphi_f\left(d_i+b_i\right)}{2J}\bar{z}_{i.1}z_{i.2} \leq -k_{i.1}\left(1-\tau_i\right)\bar{z}_{i.1}^2 \tag{49}$$

Obviously, this condition can be achieved by adjusting the parameter of $k_{i.1}$.

Based on Lemma 2, we have $-\varepsilon_i\tilde{\theta}_i\hat{\theta}_i \leq \left[\left(-\varepsilon_i\left(2\iota_i-1\right)\right)/2\iota_i\right]\tilde{\theta}_i^2 + \left(\varepsilon_i\iota_i/2\right)\theta_i{}^2$, $\iota_i > (1/2)$.

Then, according to (47) and (49), (46) can be expressed as

$$\begin{aligned}\dot{V} \leq & -\sum_{i=1}^{n}\left[\left(k_{i.1}\left(1-\tau_i\right)-\frac{l_i}{2}\right)\bar{z}_{i.1}^2-\frac{\varsigma_i}{r_i}\tilde{\theta}_i^2\right] \\ & -\sum_{i=1}^{n}\left(c_{i.1}\bar{z}_{i.1}^{\beta+1}+c_{i.2}S_{i.2}^{\beta+1}+c_{i.3}S_{i.3}^{\beta+1}\right)+n \\ & +\sum_{i=1}^{n}\sum_{m=2}^{3}\left(\frac{1}{2}\lambda_{i.m}^2+\frac{1}{2}\upsilon_{i.m}^2\right)-\sum_{i=1}^{n}\sum_{m=2}^{3}\rho_{i.m}S_{i.m}^2 \\ & -\sum_{i=1}^{n}\left(\frac{\varsigma_i}{r_i}\tilde{\theta}_i\right)^{\frac{\beta+1}{2}}+\sum_{i=1}^{n}\left(\varepsilon_i\iota_i\theta_i^2+\frac{l_i}{2}+o_{i.\delta}\right)\end{aligned} \tag{50}$$

where $\varsigma_i = r_i\left[\varepsilon_i\left(2\iota_i-1\right)/2\iota_i\right]$. If $\frac{\varsigma_i}{r_i}\tilde{\theta}_i^2 \geq 1$, we have $\left(\frac{\varsigma_i}{r_i}\tilde{\theta}_i^2\right)^{\frac{\beta+1}{2}} - \frac{\varsigma_i}{r_i}\tilde{\theta}_i^2 + \varepsilon_i\iota_i{\theta_i}^2 \leq \varepsilon_i\iota_i{\theta_i}^2$, and if $\frac{\varsigma_i}{r_i}\tilde{\theta}_i^2 < 1$, we have $\left(\frac{\varsigma_i}{r_i}\tilde{\theta}_i^2\right)^{\frac{\beta+1}{2}} - \frac{\varsigma_i}{r_i}\tilde{\theta}_i^2 + \varepsilon_i\iota_i{\theta_i}^2 \leq 1+\varepsilon_i\iota_i{\theta_i}^2$. Then, according to Lemma 3, (50) can be expressed as

$$\dot{V} \leq -\mathscr{A}V - \mathscr{B}V^{\frac{\beta+1}{2}} + \mathscr{C} \tag{51}$$

where $\mathscr{A} = \min\left\{2k_{i.1}\left(1-\tau_i\right)-l_i, 2\rho_{i.2}, 2\rho_{i.3}, 2\varsigma_i\right\}$,
$\mathscr{B} = \min\left\{c_{i.q}\cdot 2^{(\beta+1)/2}, \left(2\varsigma_i\right)^{(\beta+1)/2}\right\}$, $q = 1, 2, 3$,
$\mathscr{C} = \sum_{i=1}^{n}\sum_{m=2}^{3}\left(\frac{\lambda_{i.m}^2+\upsilon_{i.m}^2}{2}\right)+\sum_{i=1}^{n}\left(\varepsilon_i\iota_i\theta_i^2+\frac{l_i}{2}+o_{i.\delta}\right)+n$.
Based on [29], $\bar{z}_{i.1}$, $z_{i.2}$, $z_{i.3}$ can be converged in finite-time.

Moreover, to prove the stability of compensating signals ξ_i, define the Lyapunov function as

$$V_c = \frac{1}{2}\sum_{i=1}^{n}\xi_i^2 \tag{52}$$

By (19), we have

$$\begin{aligned}\dot{V}_c &= \sum_{i=1}^{n}\left[-k_{i.1}\xi_i^2 - l_i\xi_i\mathrm{sign}\left(\xi_i\right)+\xi_i\frac{3p\varphi_f\left(d_i+b_i\right)}{2J}\left(x_{i.2}^c-x_{i.2}^d\right)\right] \\ &\leq \sum_{i=1}^{n}\left[-k_{i.1}\xi_i^2 - l_i\left|\xi_i\right| + \frac{3p\varphi_f\left(d_i+b_i\right)\left|\xi_i\right|}{2J}\left|x_{i.2}^c-x_{i.2}^d\right|\right]\end{aligned} \tag{53}$$

From [28], $\left|x_{i.2}^c - x_{i.2}^d\right| \leq \lambda_i$ can be achieved in finite-time t_c, so (53) can be rewritten as

$$\dot{V}_c \leq -\mathscr{E}V_c - \left(\mathscr{F}-\sqrt{2}\hbar\right)V_c^{1/2} \tag{54}$$

where $\mathscr{E} = \min\{2k_{i.1}\}$, $\mathscr{F} = \sqrt{2}\min\left\{l_i\right\}$, $\hbar = \max\left\{\frac{3p\varphi_f(d_i+b_i)\lambda_i}{2J}\right\}$. According to [30], when $\left(\mathscr{F}-\sqrt{2}\hbar\right) > 0$, the ξ_i will be converged in finite-time.

IV.Results and Analysis

To clarify about the implementation of the proposed FDFSM-CB scheme, a multi-PMSMs HIL platform is built. The HIL platform is composed of field-programmable gate array (FPGA) and

dSPACE, which can be seen in Fig. 4. Therein, each FPGA board mainly contains a Cyclone IV E: EP4CE115F23I7 chip, several 12-bit digital to analog converter (DAC) channels and general-purpose input/output (GPIO) interfaces, and a 48MHz clock. Based on the powerful parallel computing function of FPGA, each FPGA board describes the working principle of a single inverter-PMSM system in detail, the stator voltage, current, angular speed, electromagnetic torque are calculated in real-time, and then four FPGA boards constitute a multi-PMSM system [31]. In addition, in order to make HIL results more realistic, the transistor voltage drop and inverter dead-time are also described in FPGA board. The dSPACE consists of the DS1302 I/O board and DS1202 base board, and it realizes the real-time calculation of the cooperative controller.

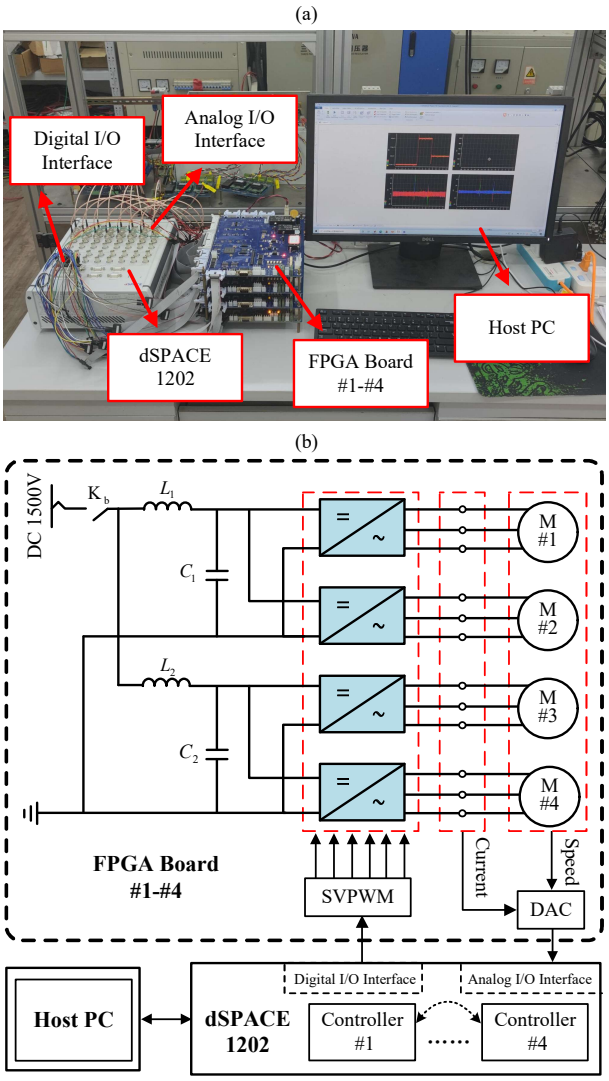

Figure 4: (a) HIL platform setup, (b) Topology of the HIL platform.

The workflow of multi-PMSMs HIL platform is as follows: 1) FPGA board #1-#4 calculate the state variables of PMSM #1-#4 according to the space vector pulse width modulation (SVPWM) signals received by GPIO interfaces; 2) DAC converts multi-channel state variables from digital signals to analog signals and then transmits them to dSPACE; 3) dSPACE realizes the data exchange of state

Table 1: Parameters of the PMSM in URT

Name	Symbol	Value
Armature resistance	R_s	$0.05\,\Omega$
Stator inductance	L_s	$2\,\text{mH}$
Permanent magnet flux	φ_f	$1/3\,\text{Wb}$
Number of poles	p	2
Equivalent inertia	J	$0.033\,\text{kg}\cdot\text{m}^2$
Viscous friction coefficient	F	$0.0003\,\text{Nms}$
DC catenary voltage	V_{dc}	$1500\,\text{V}$

Table 2: Parameters of cooperative control scheme in HIL platform

Parameter	Value	Parameter	Value	Parameter	Value
$k_{i.1}$	100	$c_{i.1}, c_{i.2}, c_{i.3}$	30	β	0.35
l_i	0.1	$\Upsilon_{i.1}$	80000	$\Upsilon_{i.2}$	200
$\mu_{i.2}, \mu_{i.3}$	1000	$\rho_{i.2}, h_{i.2}$	30000	$\rho_{i.3}, h_{i.3}$	20000
$\lambda_{i.2}, \lambda_{i.3}$	0.5	r_i	10	ε_i	0.005
$\alpha_{i.2d}$	5×10^6	$\alpha_{i.1d}$	10000		

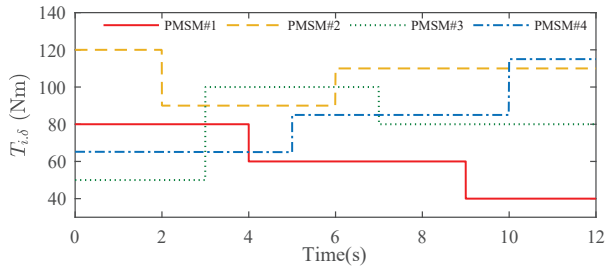

Figure 5: Load disturbance of multi-PMSMs.

variables between controllers #1-#4 according to the established directed communication topology, and constructs the neighborhood synchronization error; 4) dSPACE calculates the output of controllers #1-#4 and generate SVPWM signals, then input them into GPIO interfaces of FPGA boards.

The established directed-graph is shown in Fig. 3. The fuzzy membership functions are selected as $\kappa_i^j = \exp\left[-(x_i - o)^2/2\right]$, $i = 1, 2, 3$, $j = 1, 2, ..., 5$, $o = -2, -1, 0, 1, 2$. The parameters of the PMSM and the cooperative control scheme are listed in Table 1 and Table 2, respectively. The sampling time is selected as 100μs, the turn-on voltage drop of insulated gate bipolar transistor (IGBT) and diode are set to 1.8V and 0.7V respectively, the dead-time of the inverter is set to 2μs.

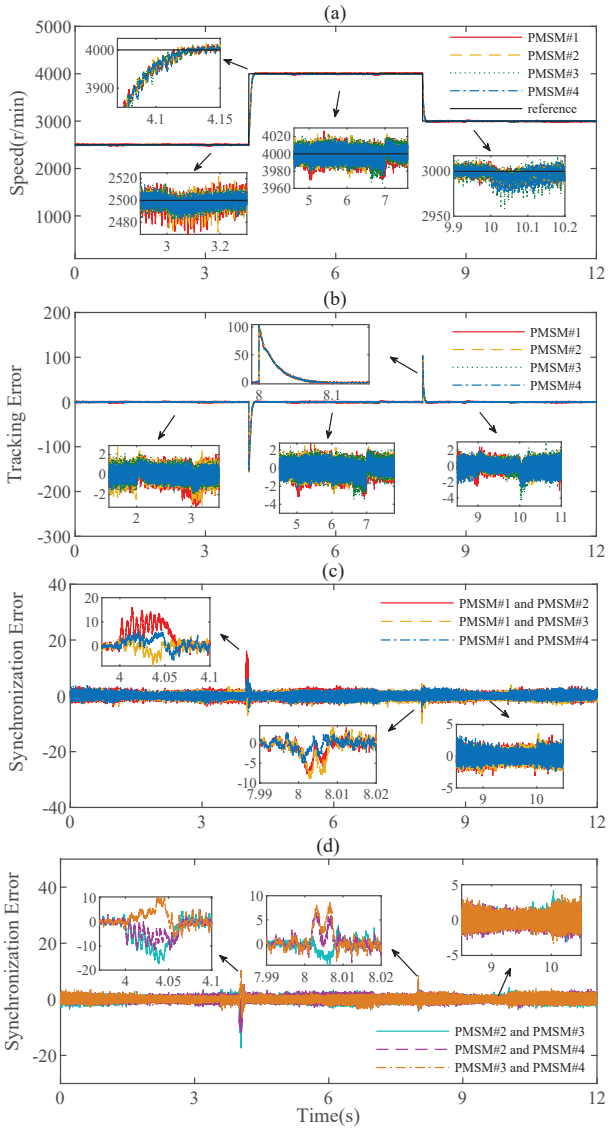

Figure 6: FDFSM-CB for multi-PMSMs: (a) Reference and actual speed, (b) Tracking errors of each PMSM, (c) Synchronization error between PMSM#1 and PMSM#2/#3/#4, (d) Synchronization error between PMSM#2, PMSM#3 and PMSM#4.

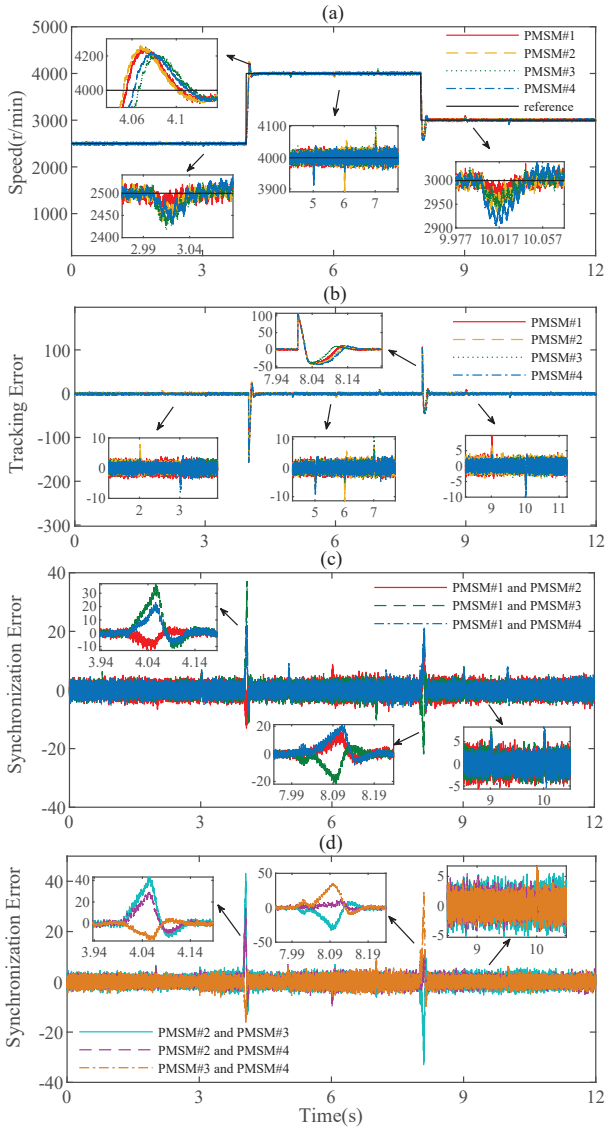

Figure 7: Method in [13] for multi-PMSMs: (a) Reference and actual speed, (b) Tracking errors of each PMSM, (c) Synchronization error between PMSM#1 and PMSM#2/#3/#4, (d) Synchronization error between PMSM#2, PMSM#3 and PMSM#4.

Remark 3: To verify the superiority of the FDFSM-CB scheme, the control performance is compared with the cooperative scheme in [13]. At present, PID cooperative controllers based on electrical coupling are mostly used in actual low-speed URT trains. Moreover, from the dynamic model of PMSM, it can be seen that PMSM has the characteristics of strong coupling, uncertainty and nonlinearity. Reference [13] propose a PID theory and design method for a class of multi-agent uncertain nonlinear systems, this is the same as the characteristics of the PMSM studied in this paper. For the above reasons, the control scheme in [13] is cited as the comparison scheme.

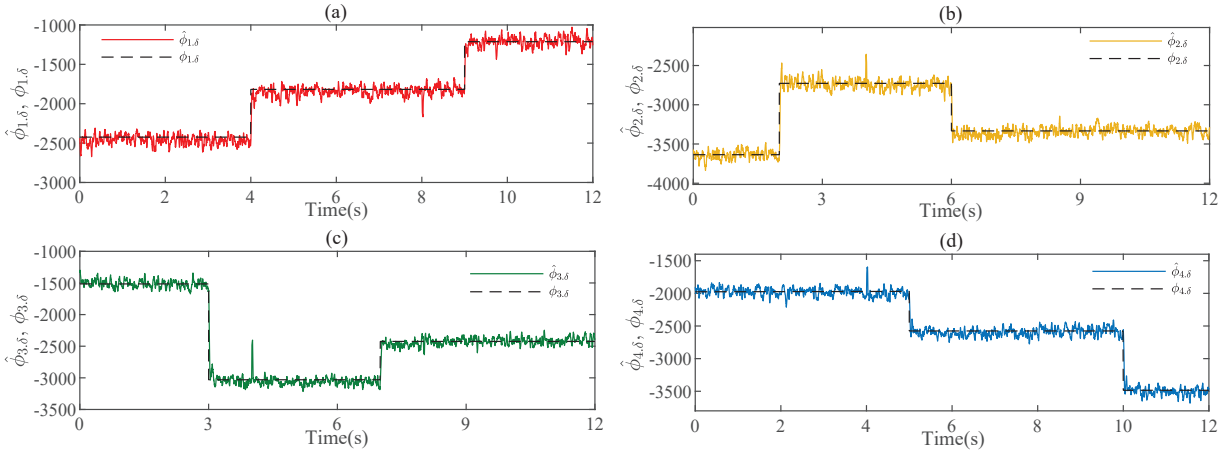

Figure 8: Actual and estimated disturbance: (a) PMSM#1, (b) PMSM#2, (c) PMSM#3, (d) PMSM#4.

The load torque disturbances of four PMSMs are considered to verify synchronization and anti-disturbance performance of the multi-PMSMs, which are shown in Fig. 5. The reference angular speed is set as a step signal to simulate the instantaneous acceleration and braking of low-speed URT. The HIL result analysis of speed tracking performance and synchronization error accuracy under the two control strategies are shown in Fig. 6 and Fig. 7. The proposed FDFSM-CB scheme has better dynamic and steady performance. In Fig. 6 (a)-(b) and Fig. 7 (a)-(b), it can be seen the control method in [13] has significant overshoot, and the proposed method has almost no overshoot. Moreover, when the load disturbances suffer abrupt changes, the proposed scheme can suppress the influence of the disturbance on the tracking trajectory more effectively, and the tracking error can be stabilized within an extremely brief period. The HIL results of synchronization error comparison are shown in Fig. 6 (c)-(d) and Fig. 7 (c)-(d). It is found that the FDFSM-CB scheme can offer a smaller synchronization error compared with the control method in [13]. Especially when the reference signal is stepped, this advantage is more obvious.

The reference disturbance and estimated disturbance are shown in Fig. 8. In the face of the applied load disturbance, the proposed DO can observe the load torque quickly and accurately, which effectively compensates the change of load torque.

To verify the robustness under uncertain PMSM parameters, the following tests are designed. In FPGA boards, the stator resistance, stator inductance and magnetic flux linkage of PMSMs are set as $R_s' = 1.2R_s, L_s' = 0.8L_s, \varphi_s' = 0.85\varphi_s$ to simulate the uncertainty of parameters. Then, the control performance between the proposed FDFSM-CB scheme and the FDFSM-CB without FLS is compared. Fig. 9 illustrates the control performance of FDFSM-CB scheme under uncertain PMSM parameters. Due to the proposed FDFSM-CB scheme uses FLSs to approximate the nonlinear dynamics of the PMSM dynamic model, thus the FDFSM-CB scheme is not sensitive to the uncertain parameters. On the contrary, Fig. 10 shows the control performance of FDFSM-CB scheme without

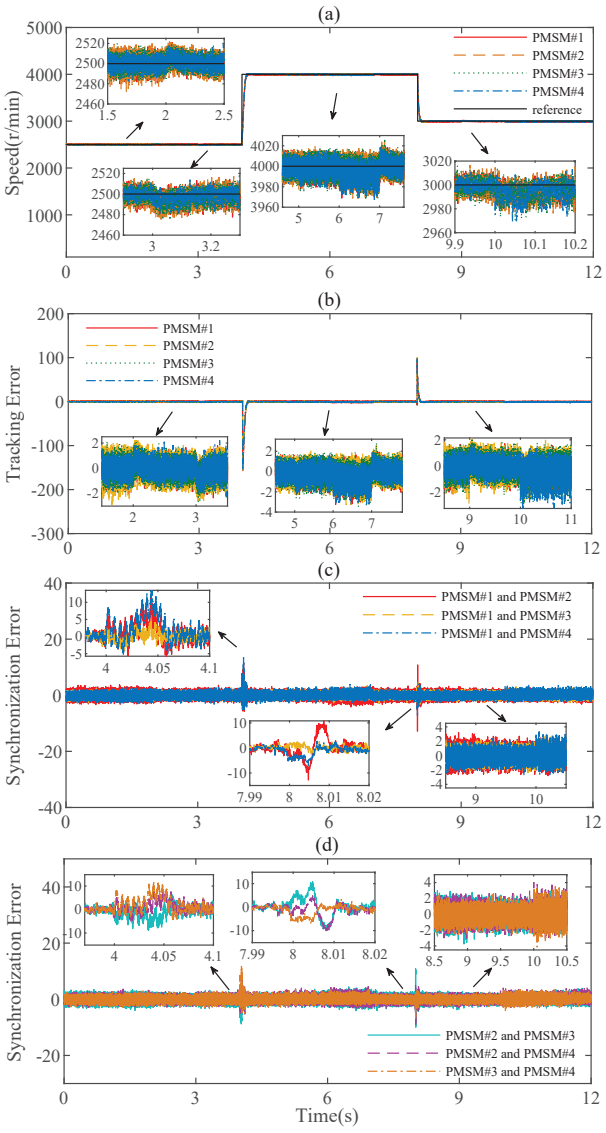

Figure 9: FDFSM-CB scheme under uncertain PMSM parameters: (a) Reference and actual speed, (b) Tracking errors of each PMSM, (c) Synchronization error between PMSM#1 and PMSM#2/#3/#4, (d) Synchronization error between PMSM#2, PMSM#3 and PMSM#4.

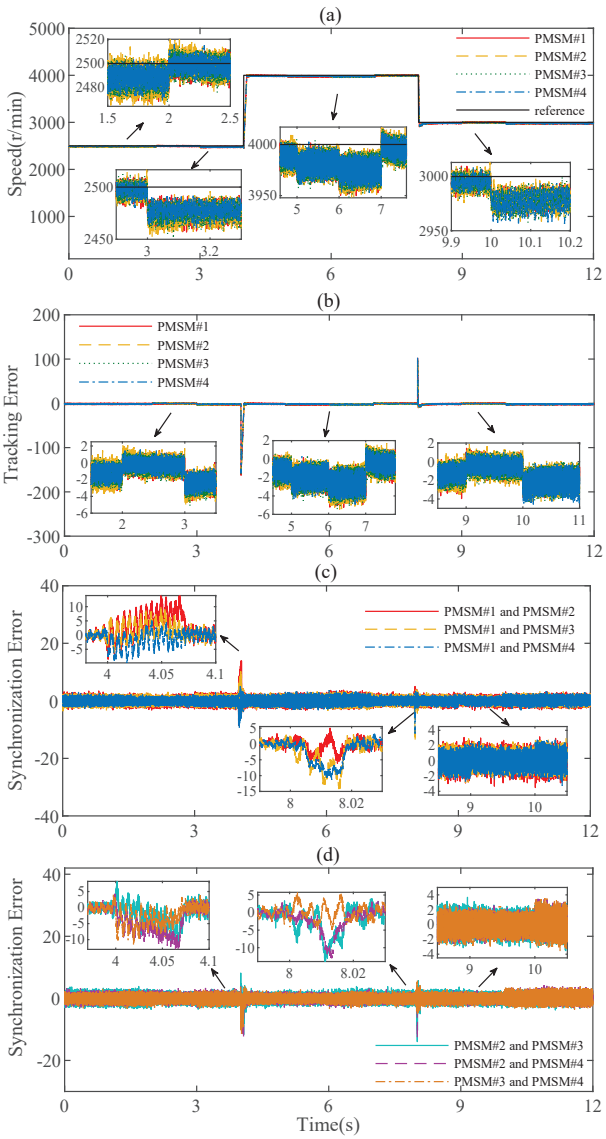

Figure 10: FDFSM-CB scheme without FLS under uncertain PMSM parameters: (a) Reference and actual speed, (b) Tracking errors of each PMSM, (c) Synchronization error between PMSM#1 and PMSM#2/#3/#4, (d) Synchronization error between PMSM#2, PMSM#3 and PMSM#4.

FLS under uncertain PMSM parameters. It can be seen that the influence of parameter uncertainty on synchronization error is not obvious, but tracking error will deviate slightly during operation and disturbance, which makes the speed unable to accurately track the reference speed. This is because the controller cannot get accurate dynamic model information. In conclusion, the robustness of the proposed controller under uncertain PMSM parameters is verified.

The influence of communication delay and communication interruption on the robustness of the con-

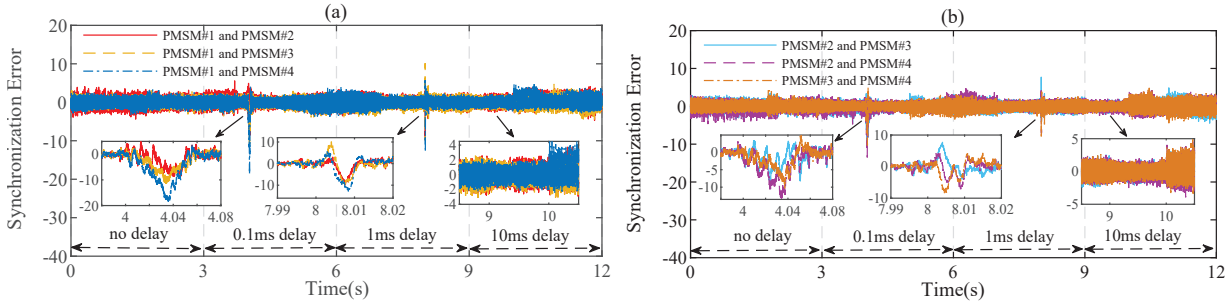

Figure 11: The influence of communication delay: (a) Synchronization error between PMSM#1 and PMSM#2/#3/#4, (b) Synchronization error between PMSM#2, PMSM#3 and PMSM#4.

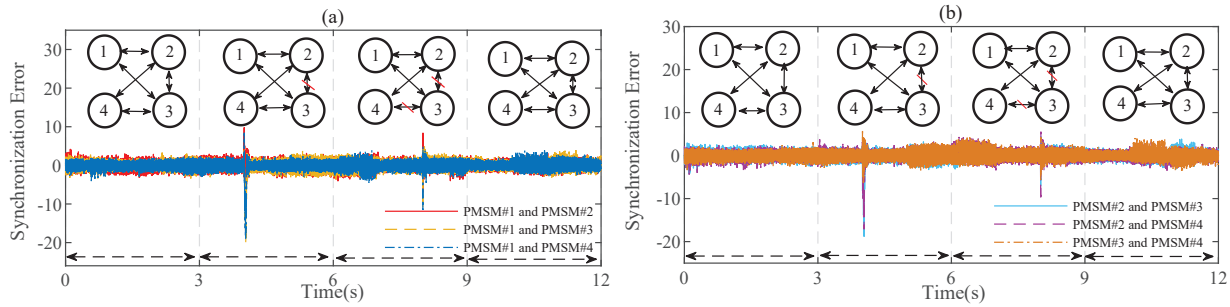

Figure 12: The influence of communication interruption: (a) Synchronization error between PMSM#1 and PMSM#2/#3/#4, (b) Synchronization error between PMSM#2, PMSM#3 and PMSM#4.

troller is studied in Fig. 11 and Fig. 12. It is shown that when the delay increases to 0.1ms, 1ms, and 10ms, the synchronization errors can still be kept within a relatively small range. Only when the URT accelerates or decelerates instantaneously, there is a slightly visible increase in synchronization errors. However, the synchronization errors are much lower than the method in [13]. In addition, the performance of the controller will not change significantly due to communication interruption. Therefore, it can be concluded that, in the face of communication degradation, the proposed FDFSM-CB scheme has better robustness.

V.Conclusion

In this paper, a speed cooperative control scheme is proposed for multi-PMSMs in low-speed URT, that tries to reduce the neighborhood synchronization error and improve the anti-disturbance performance. First, each PMSM is regarded as an agent, and the multi-PMSMs system is considered as a MAS. The information of adjacent PMSMs can be transmitted through the communication topology network, which ensures the response consistency of each PMSM. Then, considering the influence of load disturbance on synchronization accuracy, a finite-time DO is designed to provide estimated disturbance information to the controller in finite-time. Moreover, the FLSs are used to reduce the dependence of control effect on the accuracy of dynamic model, and the SOSMD is designed to re-

duce the noise caused by the direct derivation of virtual control law. Finally, the system is proved to be finite-time stable. The HIL validation results show that the multi-PMSMs under the proposed FDFSM-CB control scheme has better dynamic tracking performance with no overshoot, faster convergence. In terms of cooperative performance, the proposed control scheme has higher synchronization accuracy, and when the disturbance occurs, the synchronization state of each PMSM can be restored faster. Moreover, the robustness under uncertain PMSM parameters is verified. In our future works, a real high-power multi-PMSMs experimental platform will be built. Meanwhile, the control method will be combined with flux weakening algorithm and applied to high-speed trains.

References

[1] G. Wang, X. Hao, N. Zhao, G. Zhang, and D. Xu, "Current sensor fault-tolerant control strategy for encoderless PMSM drives based on single sliding mode observer," *IEEE Transactions on Transportation Electrification*, vol. 6, no. 2, pp. 679-689, 2020.

[2] G. Niu, J. Jiang, B. D. Youn, and M. Pechtc, "Autonomous health management for PMSM rail vehicles through demagnetization monitoring and prognosis control," *ISA Transactions*, vol. 72, pp. 245-255, 2018.

[3] R. Thike, and P. Pillay, "Mathematical model of an interior PMSM with aligned magnet and reluctance torques," *IEEE Transactions on Transportation Electrification*, vol. 6, no. 2, pp. 647-658, 2020.

[4] M. H. Cheng, Y. J. Li, and E. G. Bakhoum, "Controller synthesis of tracking and synchronization for multiaxis motion system," *IEEE Transactions on Control Systems Technology*, vol. 22, no. 1, pp. 378-386, 2014.

[5] Y. Yang, C. Hua and X. Guan, "Adaptive fuzzy finite-time coordination control for networked nonlinear bilateral teleoperation system," *IEEE Transactions on Fuzzy Systems*, vol. 22, no. 3, pp. 631-641, 2014.

[6] Z. Zhang, K. T. Chau, and Z. Wang, "Chaotic speed synchronization control of multiple induction motors using stator flux regulation," *IEEE Transactions on Magnetics*, vol. 48, no. 11, pp. 4487-4490, 2012.

[7] F. Lin, P. Chou, C. Chen and Y. Lin, "DSP-based cross-coupled synchronous control for dual linear motors via intelligent complementary sliding mode control," *IEEE Transactions on Industrial Electronics*, vol. 59, no. 2, pp. 1061-1073, 2012.

[8] D. Zhao, C. Li, and J. Ren, "Speed synchronisation of multiple induction motors with adjacent cross-coupling control," *IET Control Theory and Application*, vol.4, no.1, pp.119-128, 2010.

[9] T. Shi, H. Liu, Q. Geng, and C. Xia, "Improved relative coupling control structure for multi-motor speed synchronous driving system," *IET Electric Power Applications*, vol. 10, no. 6, pp. 451-457, 2016.

[10] D. Xu, W. Zhang, P. Shi, and B. Jiang, "Model-free cooperative adaptive sliding-mode-constrained-control for multiple linear induction traction systems," *IEEE Transactions on Cybernetics*, vol. 50, no. 9, pp. 4076-4086, 2020.

[11] K. Zhang, B. Jiang, and P. Shi, "Adjustable parameter-based distributed fault estimation observer design for multiagent systems with directed graphs," *IEEE Transactions on Cybernetics*, vol. 47, no. 2, pp. 306-314, 2017.

[12] Y. Lv, Z. Li, and Z. Duan, "Distributed PI control for consensus of heterogeneous multiagent systems over directed graphs," *IEEE Transactions on Systems, Man, and Cybernetics: Systems*, vol. 50, no. 4, pp. 1602-1609, 2020.

[13] J. Zhang, and L. Guo, "Theory and design of PID controller for nonlinear uncertain systems," *IEEE Control Systems Letters*, vol. 3, no. 3, pp. 643-648, 2019.

[14] Q. Ma, "Cooperative control of multi-agent systems with unknown control directions," *Applied Mathematics and Computation*, vol. 292, pp. 240-252, 2017.

[15] H. R. Chamorro, M. Nazari, D. Babazadehi, N. R. Malik and M. Ghandhari, "Consensus control for induction motors speed regulation," *2014 16th European Conference on Power Electronics and Applications*, 2014, pp. 1-6.

[16] B. Ding, D. Xu, B. Jiang, P. Shi, and W. Yang, "Disturbance-observer-based terminal sliding mode control for linear traction system with prescribed performance," *IEEE Transactions on Transportation Electrification*, vol. 7, no. 2, pp. 649-658, 2021.

[17] X. Zhang, B. Hou and Y. Mei, "Deadbeat predictive current control of permanent-magnet synchronous motors with stator current and disturbance observer," *IEEE Transactions on Power Electronics*, vol. 32, no. 5, pp. 3818-3834, 2017.

[18] S. Lin, Y. Cai, B. Yang, and W. Zhang, "Electrical line-shafting control for motor speed synchronisation using sliding mode controller and disturbance observer," *IET Control Theory and Applications*, vol. 11, no. 2, pp. 205-212, 2017.

[19] F. Bayat, S. Mobayen, and S. Javadi, "Finite-time tracking control of nth-order chained-form non-holonomic systems in the presence of disturbances," *ISA Transactions*, vol.63, pp. 78-83, 2016.

[20] Y. Jiang, W. Xu, C. Mu and Y. Liu, "Improved deadbeat predictive current control combined sliding mode strategy for PMSM drive system," *IEEE Transactions on Vehicular Technology*, vol. 67, no. 1, pp. 251-263, 2018.

[21] Y. Dai, S. Ni, D. Xu, L. Zhang, and X. Yan, "Disturbance-observer based prescribed-performance fuzzy sliding mode control for PMSM in electric vehicles," *Engineering Applications of Artificial Intelligence*, vol. 104, 2021.

[22] Q. Shen, P. Shi, J. Zhu, S. Wang, and Y. Shi, "Neural networks-based distributed adaptive control of nonlinear multi-agent systems," *IEEE Transactions on Neural Networks and Learning Systems*, vol. 31, no. 3, pp. 1010-1021, 2020.

[23] L. Zhao, J. Yu, and C. Lin, "Distributed adaptive output consensus tracking of nonlinear multi-agent systems via state observer and command filtered backstepping," *Information Sciences*, vol. 478, pp. 355-374, 2019.

[24] J. Yu, P. Shi, W. Dong, and H. Yu, "Observer and command-filter-based adaptive fuzzy output feedback control of uncertain nonlinear systems," *IEEE Transactions on Industrial Electronics*, vol. 62, no. 9, pp. 5962-5970, 2015.

[25] L. Zhao, J. Yu, C. Lin, and Y. Ma, "Adaptive neural consensus tracking for nonlinear multiagent systems using finite-time command filtered backstepping," *IEEE Transactions on Systems, Man, and Cybernetics: Systems*, vol. 48, no. 11, pp. 2003-2012, 2018.

[26] X. Huang, W. Lin, and B. Yang, "Global finite-time stabilization of a class of uncertain nonlinear systems" *Automatica*, 41, no. 5, pp. 881-888, 2005.

[27] J. A. Moreno, and M. Osorio, "Strict lyapunov functions for the super-twisting algorithm," *IEEE Transactions on Automatic Control*, vol. 57, no. 4, pp. 1035-1040, 2012.

[28] A. Levant, "Higher-order sliding modes, differentiation and output feedback control," *International Journal of Control*, vol. 76, no. 9-10, pp. 924-941, 2003.

[29] J. Yu, P. Shi, and L. Zhao, "Finite-time command filtered backsteppingcontrol for a class of nonlinear systems," *Automatica*, vol. 92, pp. 173-180, 2018.

[30] S. Yu, X. Yu, B. Shirinzadeh, and Z. Man, "Continuous finite-time control for robotic manipulators with terminal sliding mode," *Automatica*, vol. 41, no. 11, pp. 1957-1964, 2005.

[31] L. Zhang, J. Liu, W. Qi, Q. Chen, R. Long, and S. Quan, "A parallel modular computing approach to real-time simulation of multiple fuel cells hybrid power system," *International Journal of Energy Research*, vol. 43, no. 10, pp. 5266-5283, 2019.